ISTAM

Israel Society for Theoretical and Applied Mechanics

האגוד הישראלי למכניקה עיונית ושימושית

An Adhering Organization of the
International Union of Theoretical and Applied Mechanics
(IUTAM: http://www.iutam.net)

ISTAM ANNUAL SYMPOSIUM

TECHNICAL PROGRAM

1 December 2013 | Tel Aviv University

ISTAM 2013 Annual Symposium Program

Location: Rosenblatt Auditorium, Computer and Software Engineering Building, Tel Aviv University

09:30 – 09:50 Registration and coffee

09:50 – 10:00 *Opening:* **MB Rubin**

General Session Chairman: **I Harari**, Tel Aviv University

10:00 – 10:20 **H Chai** - Tel Aviv University, *"On crack tip shielding by micro cracking in biological structures."*

10:20 – 10:40 **MM Safadi** and MB Rubin - Technion, *"Modeling rate-independent hysteresis in large deformations of preconditioned soft tissues."*

10:40 – 11:00 **I Gelfeld,** G Davidi and J Tirosh - Technion, *"Quantifying damages in autofrettaged thick walled tubes."*

11:00 – 11:20 **I Hotzen**, O Ternyak, S Shmulevich and D Elata - Technion, *"Novel Motion Conversion Mechanisms in MEMS."*

11:20 – 11:40 **A Lisyansky**, Y Starosvetsky - Technion, *"Effective Particles Approximation of a Primary Pulse Transmission in Hexagonally Packed, Damped Granular Crystal with a Spatially Varying Cross Section: Analytical Study."*

11:40 – 12:00 **Y Toledo** - Tel Aviv University, *"The oblique parabolic equation model for linear and nonlinear wave shoaling."*

12:00 – 13:20 Lunch

Special MicroFluidic Session I Chairman: **Y Feldman**, Ben Gurion University

13:20 – 13:40 **E Afik** - Weizmann, *"Robust and Highly Performant Ring Detection Algorithm for 3d Particle Tracking Using 2d Microscope Imaging."*

13:40 – 14:00 **O Manor**, A Rezk, JR Friend and LY Yeo - Technion, *"A generalized view of high frequency substrate vibration induced wetting (Acoustowetting)."*

14:00 – 14:20 **Y Green** and G Yossifon - Technion, *"On the Effects of 3D Field Focusing at a Heterogeneous Permselective Surface on Concentration Polarization."*

14:20 – 14:40 Q Li, K Anupindi, Y Delorme, **SH Frankel** - Technion, *"High-Order Numerical Simulations of Electrokinetic Instability in a Cross-shaped Microchannel."*

14:40 – 15:00 **A Boymelgreen**, G Yossifon and T Miloh - Technion, *"Frequency dispersion in dipolophoresis of metallodielectric Janus spheres."*

15:00 – 15:20 *Break*

Special MicroFluidic Session II Chairman: **SH Frankel**, Technion

15:20 – 15:40 **H Stauber,** R Fishler, P Hofemeier, D Waisman, and J Sznitman - Technion, *"Dispersion Phenomena of Fine Particles in Pulmonary Alveolar Capillary-Inspired Networks."*

15:40 – 16:00 J Shemesh, T Ben Arye, **J Avesar**, JH Kang, A Fine, M Super, A. Meller, D.E. Ingber, S. Levenberg - Technion, *"Nanodroplet array for multiplexed single-cell assays."*

16:00 – 16:20 **SB Elbaz** and AD Gat - Technion, *"Dynamics of an Elastic Cylinder Containing a Viscous Liquid with Application to Soft Robotics."*

16:20 – 16:40 **E Keinan**, E Ezra, Y Nahmias - Hebrew University, *"Frame Rate Free Image Velocimetry for Microfluidic Devices."*

16:40 – 17:00 R Fishler, MK Mulligan, and **J Sznitman** - Technion, *"Acinus-on-a-chip: a microfluidic platform for pulmonary acinar flows."*

The annual membership fee to ISTAM is 100 NIS. It includes the lunch at the symposium and can be paid during the registration.

All lectures are open to the public free of charge

Table of Contents

On crack tip shielding by micro cracking in biological structures

Herzl Chai
School of Mechanical Engineering, Faculty of Engineering, Tel Aviv University
herzl@eng.tau.ac.il

Biological load-bearing structures are often characterized by layered material architecture which is composed of stiff mineral layers held together by a soft organic matrix. Under external loading various fracture modes may occur including transverse cracking within the stiff layers and delamination at the interface between the stiff and soft materials. Often the latter fracture may originate from multiple channel or tunnel cracks in the hard layers. Interestingly, such multiple cracks may provide a beneficial stress shielding effect that would retard or inhibit further fracture growth, whether it may be delamination or crack penetration into the softer material phase. Although this subject has been addressed quite extensively in relation to ceramics materials, little is known on the actual process of fracture. Moreover, recently such an effect has been found to operate also in biological structure such as teeth and dental restorations, which greatly extend the scope of this basic problem. Teeth are composed of a thin, hard protective layer (enamel) which is supported a soft dentin substrate. As shown in Fig. 1a, under occlusal loading multiple rather than a single crack emanate from preexisting flaws called tufts. A simple fracture mechanics analysis of this condition (Fig. 1b) reveals a drastic reduction in the stress intensity factor at the tip of the transverse cracks due to the presence of adjacent cracks.

We observe the evolution of transverse cracking and delamination damage in-situ for a number of systems of current interest including an all-transparent glass/epoxy bilayer, some dental restorations such as porcelain/Y-TZP, and extracted human teeth. The effect of crack tip stress shielding on the growth of delamination and/or transverse cracks is evaluated using a 2D FEA. The analysis predicts general trends observed in the tests, and it indicates means for an optimal design against premature failure.

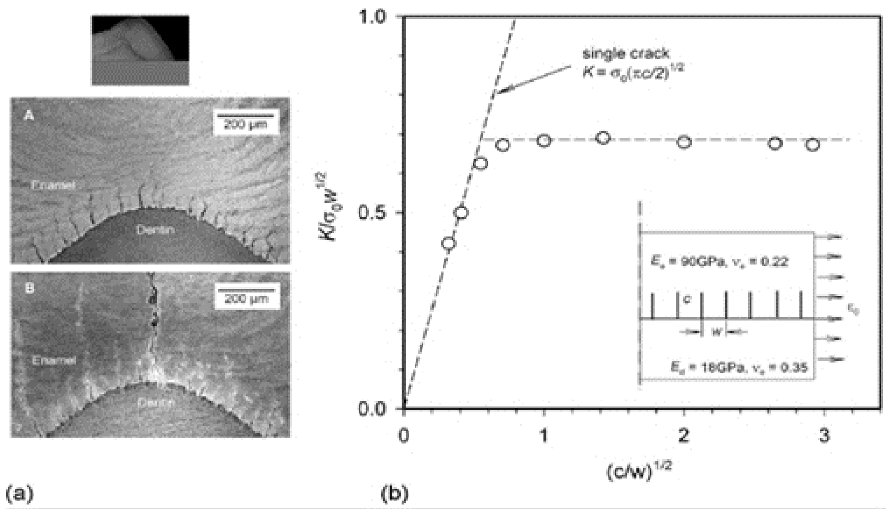

Fig. 1.: Stress shielding effect in dental enamel; (a) - multiple cracks grow from preexisting defect called tufts in the dentin/enamel junction, (b) – a FEA showing how the stress intensity factor at the crack tip is reduced by the addition of adjacent cracks.

Keywords
Layered structure, delamination, transverse cracks, stress shielding.

References

H. Chai and Y. Fox, “On delamination growth from channel cracks in thin-film coatings”, International Journal of Solids and Structures 2012; 48:1092–1100.

B.R. Lawn, H. Chai, A. Barani and M.B. Bush, “Transverse fracture of canine teeth”. Journal of Biomechanics, 2013; 46:1561-1567.

H. Chai, J.J-W. Lee, P.J. Constantino, P.W. Lucas and B.R. Lawn, “Remarkable resilience of teeth”, Proceedings of the National Academy of Science 2009;106:7289–7293.

Acknowledgments
The work was supported by the Israeli Science Foundation [ISF Grant 810/09].

Modeling rate-independent hysteresis in large deformations of preconditioned soft tissues

MM Safadi* and MB Rubin

Faculty of Mechanical Engineering, Technion - Israel Institute of Technology

*safadi@tx.technion.ac.il

In general, the material response of biological soft tissues is isochoric, rate-dependent and inelastic. Specifically, the stress-strain behavior of the tissue when subjected to cyclic loading at a constant strain rate between fixed stress or strain limits exhibits time-dependent inelastic hysteresis loops that shift with each cycle towards a steady-state hysteresis loop. It was experimentally observed that this steady-state hysteresis loop is relatively insensitive to the magnitude of the constant strain rate over a wide range of strain rates. This steady-state hysteresis loop characterizes the state of the material, which is referred to as preconditioned, and the transitional process towards this preconditioned state is referred to as preconditioning. The most common model used in the literature to characterize the dissipation of the hysteresis loop of a preconditioned tissue is referred to as pseudo-elasticity (Fung, 1993; Ogden and Roxburgh, 1999). In particular, Dorfmann et al. (2008) exploited this approach to characterize the response of muscle tissue, however, the notion of loading and unloading in their model is unclear.

The objective of this work is to develop simple isotropic constitutive equations for large deformations of preconditioned soft tissues within the framework of plasticity theory, which are valid for general loading histories and include dissipation. Specifically, the preconditioned tissue is modeled as a composite of a hyperelastic component and an inelastic (dissipative) component such that the Cauchy stress can be expressed in the additive form

$$\boldsymbol{T} = \boldsymbol{T}_e + \boldsymbol{T}_d = -p\,\boldsymbol{I} + 2\mu_e(\beta_1 - 3)^{n_e}\boldsymbol{g}'' + 2\mu_d(\alpha_1 - 3)^{n_d}\boldsymbol{g}_e'' \quad ,$$
$$\beta_1 = \boldsymbol{B}' \cdot \boldsymbol{I} \quad , \quad \alpha_1 = \boldsymbol{B}_e' \cdot \boldsymbol{I} \quad , \quad \boldsymbol{g}'' = \frac{1}{2}\boldsymbol{B}'' \quad , \quad \boldsymbol{g}_e'' = \frac{1}{2}\boldsymbol{B}_e''$$

where p is the pressure, $\{\boldsymbol{g}'', \boldsymbol{g}_e''\}$ represent total and elastic distortional strains, respectively, and $\{\mu_e, \mu_d\}$ are non-negative constants having the units of stress. Furthermore, the inelastic component is modeled as an elastic-plastic material using a yields function of the form

$$g = \gamma_e - \kappa \leq 0 \quad , \quad \gamma_e = \sqrt{\frac{3}{2}\boldsymbol{g}_e'' \cdot \boldsymbol{g}_e''}$$

where γ_e is a measure of elastic distortion and κ is the hardening variable, with elastic material response when $g < 0$. Moreover, a distinction is made between deformation loading/unloading and inelastic loading/unloading, with the hardening variable κ having different functional forms for inelastic loading and unloading. Figure 1 shows that the model predictions of the engineering stress Π_{11} as a function of the axial stretch λ compare well with the experimental stress data for a preconditioned Manduca muscle in (Dorfmann et al., 2008).

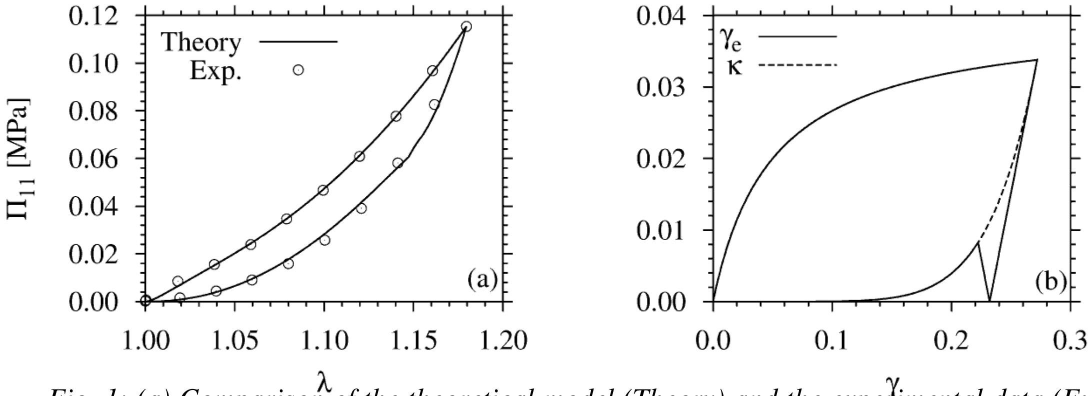

Fig. 1: (a) Comparison of the theoretical model (Theory) and the experimental data (Exp.) in (Dorfmann et al. 2008). (b) Response of the hardening variable κ *and the measure of elastic distortional deformation* γ_e.

References

Dorfmann, A. L., Woods, W. A., Trimmer, B. A., 2008. Muscle performance in a soft-bodied terrestrial crawler: constitutive modelling of strain-rate dependency. Journal of The Royal Society Interface 5 (20), 349–362.

Fung, Y. C., 1993. Biomechanics: Mechanical Properties of Living Tissues. Springer.

Ogden, R. W., Roxburgh, D. G., 1999. A pseudoelastic model for the mullins effect in filled rubber. Proceedings of the Royal Society of London. Series A: Mathematical, Physical and Engineering Sciences 455 (1988), 2861–2877.

Quantifying damages in autofrettaged thick walled tubes

I. Gelfeld*, G. Davidi and J. Tirosh
Faculty of mechanical engineering, Technion
*irene.gelfeld@gmail.com

A practical manufacturing process, called 'autofrettage', intends to imbed purposely residual stresses in certain axi-symmetric pipe-like structures (thick wall tubes, pressure vessels, etc.) to enhance their capability to withstand elevated stresses that otherwise would cause failure. The core idea is to over-pressurize momentarily the structure,(herewith, a thick-wall tube) in order to generate a certain amount of plasticity around the inner diameter. Upon unloading back to zero-pressure, the associated relief of the elastic stresses 'pushes away' the plastic layer (totally or partially) which leads to *a highly favorable distribution of residual stresses in the tube* (to be discussed lengthily during the presentation).

While repeating briefly the analysis of this long-standing procedure, we have tried to add apparently new rigor-analytical features: (a) quantifying the loosing ability to sustain elevated stresses as may occur *when the inner bore of the tube faces geometrical changes* (like removing a thin layer from the bore diameter or grooving trajectories inside the bore, etc.). (b) reformulating the induced residual stresses and the possible damage mentioned above, based on von-Mises yielding criterion rather than the less general Tresca's criterion used mostly hitherto.

In parallel, the offered solutions for the features (a) and (b) are compared to an independent numerical solutions (using FEM with ANSYS code) indicating a highly satisfactory agreement.

An example of the results is shown below:

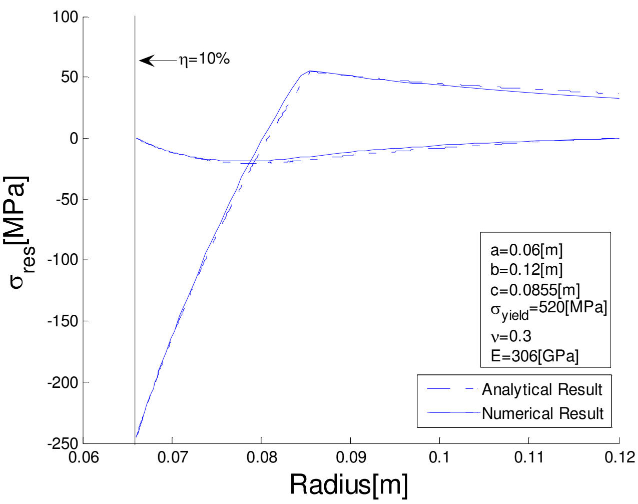

Fig 1.: Comparison of the analytical vs. the numerical solution (using FEM) of the two residual stress components (radial and circumferential) for very short tube (namely, under plain stress condition) after removing a thin layer (of 10%) from the inner bore 'a' of the tube.

Note that the radial stress component is always under compression (satisfying zero level at the boundaries).The circumferential stress (the tangential component of stress) is under relatively high compression at the inner bore surface. It changes gradually to tensile stress. The highest tensile point is located at the place where the elastic-plastic border was situated during the activation of the over-pressure in the autofretage process.

Acknowledgments
The work is based on the M.Sc of the first author while being in 'BRAKIM' undergraduate program in the Faculty of Mechanical Engineering at the Technion.

(*) Serving now in IDF.

Novel Motion Conversion Mechanisms in MEMS

I. Hotzen, O. Ternyak, S. Shmulevich and D. Elata
Technion - Israel Institute of Technology, Israel
*inbar28@gmail.com

We present for the first time ever, a novel motion conversion mechanism which is compatible with standard mass-fabrication micromachining. The new mechanism is designed to linearly convert in-plane to out-of-plane motion. The mechanism is constructed from pairs of parallel beams of two different heights. Motion conversion is achieved by fastening together each pair of beams by a small number of rigid connectors [1]. These rigid connectors stiffen the in-plane response of the mechanism, but induce an out-of-plane motion. With a new test device, we show that the ratio of motion conversion is increased when more connectors are used. In a different test device, we demonstrate parallel out-of-plane motion of a flat stage, achieved by the new conversion mechanism.

In-plane electrostatic comb-drive actuation is a well established technology, which offers linearity over a large range of motion [2, 3]. Out-of-plane electrostatic actuation, often requires complex fabrication and assembly processes, and suffers from nonlinear effects. To this end, motion conversion mechanisms were introduced, which harness the well established in-plane actuation to achieve well controlled out-of-plane motion [4]. These mechanisms are constructed from beams with slanted cross-sections (Fig. 1), while the in-plane comb-drive actuators are constructed from beams with vertical cross-sections. Combination of elements with slanted and with vertical cross-sections, is incompatible with mass-fabrication technology [5].

The new motion conversion mechanism is based on beams of two different heights, which are linked together by stiffening connectors (Fig. 2). Effectively, the dual-height cross-section (Fig. 2) is similar to the slanted cross section, in the sense that its principal second-moment axes are tilted. However, the dual-height structure cross-section can be micromachined using standard DRIE milling with one additional step for producing recessed beams [6]. Figure 2 shows a perspective of the new mechanism, without the actuating comb-drives (and an inset of the top view).

A special comparison test device was fabricated with several implementations of the new conversion mechanism, each with a different number of connectors (Fig. 3). Pairs of identical conversion structures are connected to the same main shuttle which is driven in-plane. In each pair, the tips move out-of-plane: one tip moves up and the other down (inset close-ups in Fig. 3). The tip motions in each pair increases with increasing number of connectors. The motion was measured with a Veeco optical profilometer (inset in Fig. 3 of a structure with 15 connectors). The deformed state of a device, similar to the one presented in Fig. 2, with 15 connectors, is presented in Fig. 4. The central stage is connected to the new conversion mechanisms, and is uniformly elevated when in-plane motion is induced by comb-drive actuators. In the symposium we intend to present additional devices and measurements. We will also present the fabrication process, which is fully compatible with mass fabrication, and includes provisions for eliminating the effects of lithography misalignments.

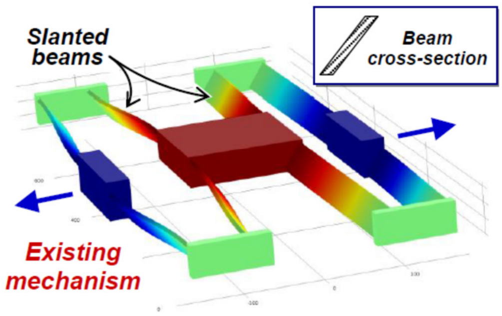

Figure 1: Motion conversion mechanism constructed from beam flexures with slanted cross-sections [4]. It is very complicated to micromachine both slanted beams and vertical structures which are necessary for comb-drive actuators (not shown). The shuttles are pulled away (blue arrows) and consequently the central stage is parallely deflected upwards (blue=level, red=maximal elevation)

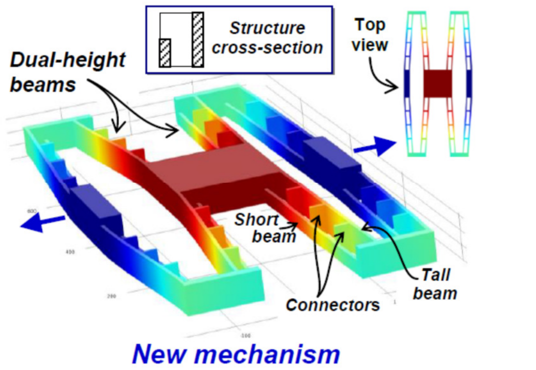

Figure 2: The new motion conversion mechanism. The dual-height beams have vertical cross-sections and are therefore fully compatible with bulk micromachining and mass-fabrication.

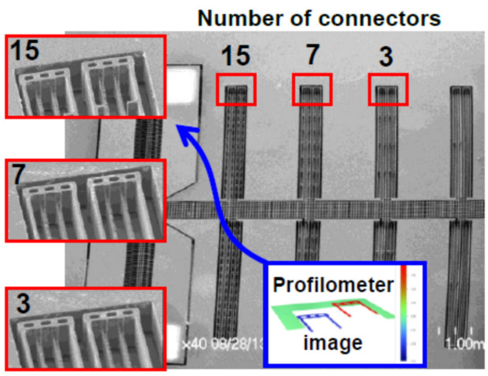

Figure 3: SEM image of a test device for comparing out-of-plane motion of structures with different number of connectors. All structures are connected to the same shuttle. In each pair of structures one moves up and the other moves down.

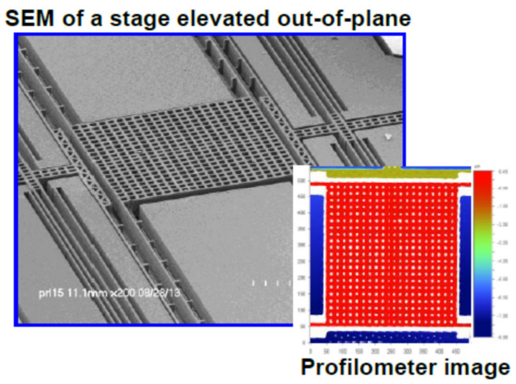

Figure 4: SEM image and a Veeco profilometer image of a device of the type presented in Fig.2. The central stage is uniformly elevated when the motion conversion mechanisms are moved in-plane.

References

[1] D. Elata and A. Hirshberg, "Motion conversion mechanisms." Patent Pend., 2013.
[2] W.C. Tang, T.H. Nguyen, and R.T. Howe, "Laterally driven polysilicon resonant microstructures," *Sensors & Actuators*, vol. 20, pp. 25-32, 1989.
[3] C. Marxer, O. Manzardo, H.P. Herzig, R. Dandliker, and N. De-Rooij, "An Electrostatic actuator with large dynamic range and linear displacement-voltage behavior for a miniature spectrometer," *Transducers 1999*, Sendai, Japan, 1999.
[4] Y. Ando, T. Ikehara, and S. Matsumoto, "Design, fabrication and testing of new comb actuators realizing three-dimensional continuous motions," *Sensors and Actuators a-Physical*, vol. 97-8, pp. 579-586, 2002.
[5] Y. Ando, "Fabrication and testing of three-dimensional stages providing displacement of up to 8 um," *IEEE-Transducers 2005*, 2005.
[6] V. Milanovic, S. Kwon, and L. P. Lee, "Monolithic vertical combdrive actuators for adaptive optics," *IEEE/LEOS Optical MEMS 2002*, 2002.

Effective Particles Approximation of a Primary Pulse Transmission in Hexagonally Packed, Damped Granular Crystal with a Spatially Varying Cross Section: Analytical Study

A. Lisyansky and Y. Starosvetsky*
Faculty of Mechanical Engineering, Technion Israel Institute of Technology
*staryuli@tx.technion.ac.il

Present study concerns the dynamics of a primary pulse propagating through the uncompressed, 2D hexagonal granular crystal with spatially varying cross section and given to onsite perturbation. This system under consideration is referred to in the paper as a fundamental model. Here we demonstrate that application of the uniform, shock like loading on the narrow end of the granular crystal leads to the formation of a spatially localized, traveling, primary pulse. At the first stage of propagation the shape of a spatial distribution of a primary pulse is nearly straight. However, this shape of a spatial distribution slowly deviates from a straight line along with its propagation (Fig.1). Thus, after sufficient number of layers, the primary pulse becomes distributed along the curve rather than a straight line. In the current work we primarily focus on the first stage of propagation of the primary pulse. Thus we show that a spatial evolution of the strongly localized primary pulse can be efficiently described by a reduced order model comprising the perturbed, purely nonlinear (Hertz interaction law) chain of effective particles with the linearly increasing masses and stiffness coefficients. Using the recently developed analytical procedure of nonlinear maps and a subsequent homogenization, we derive a closed form, analytical approximation depicting the evolution of the traveling primary pulse. It is worthwhile noting that the devised analytical approximation accounts for the presence of an onsite perturbation (e.g. dissipation) imposed on the full model. Results of the numerical simulations of the reduced order model as well as these of the analytical approximation are found to be in a spectacular agreement with the results of numerical simulations obtained for the full 2D model. Theoretical results derived for the fundamental model are further applied on a slightly different dynamical setup concerning the primary pulse transmission in the hexagonally packed, granular crystal given to an internal, radial, shock like loading. Here we show that despite the obvious differences between the two physical models under consideration, the analytical approach devised for the fundamental one provides a very good approximation also for the problem of internal, radial excitation of the perturbed, hexagonally packed, granular crystal.

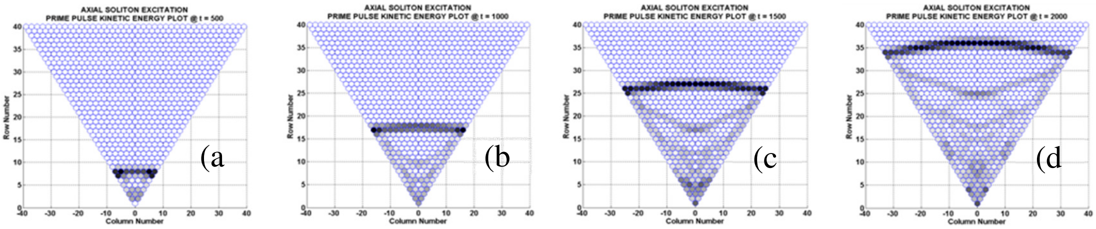

Fig. 1: 2D snapshots qualitatively depicting the relative Kinetic Energy distribution in the un-damped granular crystal subjected to the axial load (a) t =500 (b) t= 1000 (c) t =1500 (d) t= 2000.

Keywords: Granular Crystals, Nonlinear Map, Effective Particles, Primary pulse transmission

Acknowledgments

The authors are grateful to Israel Science Foundation (Grant 484 /12) for financial support

The oblique parabolic equation model for linear and nonlinear wave shoaling

Yaron Toledo
School of Mechanical Engineering, Faculty of Engineering, Tel Aviv University
toledo@tau.ac.il

Common simplified models for surface gravity waves result in parabolic type equations. These equations mostly assume a negligible refection from the bottom variations but acount for both refraction and diffraction effects. A common deffiency of these equations is an inherent assumption of normally incident waves, which cause an increasing error, as the incident waves propagate from an increasing attack angle. In the nonlinear formulation of this type of equations former works added the assumption of small crossing angles between interacting waves, which also limits the applicability of these nonlinear models to narrow directional spectra. The current work presents a parabolic approximation for oblique incident waves that over comes these limitations. This is done by introducing a perturbation solution for the wave's phase function, which in its lowest order corresponds to oblique incident waves on a bottom with no lateral changes. The resulting curved wave ray structure replaces the simplifed straight one used in the derivation process of various former models. In the non-linear model, the nonlinear interactions are calculated between the frequency modes while taking into a count the different propagating directions. Numerical results of the oblique parabolic equation show great advantages comparing to other formulations that use a straight wave-ray structure and the small crossing angles assumption. The nonlinear model was used to investigate the nonlinear shoaling of two similar monochromatic waves approaching from different angles. This fundamental nonlinear interaction problem shows that there is an energy transfer to waves of the primary harmonic that approach in larger attack angles than the two incident waves. This leads to a counter-intuitive understanding.

Unlike in the case of linear wave shoaling where the waves reduce their attack angle in the refraction process, in the nonlinear shoaling process the attack an-glecan increase. Fundamental numerical simulations of the linear and nonlinear oblique parabolic models are shown to be in excellent agreement with the originating mild-slope equations. This reassures the advantage of applying these models to various shoaling scenarios for both linear and nonlinear waves. The method is not limited to surface gravity waves and can be used in modeling acoustic waves, gravity waves in the atmosphere and other fields of physics that involve the use of parabolic equations.

Robust and Highly Performant Ring Detection Algorithm for 3d Particle Tracking Using 2d Microscope Imaging

E. Afik

Department of Physics of Complex Systems, Weizmann Institute of Science

eldad.afik@weizmann.ac.il

Three-dimensional particle tracking is an essential tool in studying dynamics under the microscope, namely, cellular trafficking, bacteria taxis, fluid dynamics in microfluidics devices. The 3d position of a fluorescent particle can be determined using 2d imaging alone, by measuring the diffraction rings generated by an out-of-focus particle, imaged on a single camera. Here I present a ring detection algorithm exhibiting a high detection rate, which is robust to the challenges arising from particles vicinity. It is capable of real time analysis thanks to its high performance and low memory footprint. Many of the algorithmic concepts introduced can be advantageous in other cases, particularly for sparse data. The implementation is based on open-source and cross-platform software packages only, making it easy to distribute and modify. The image analysis algorithm, which is an offspring of the full 3d circle Hough transform, addresses the need to efficiently trace the trajectories of several particles concurrently, when their number in not necessarily fixed, by solving a classification problem. The current implementation is robust to ring occlusion, inclusions and overlaps, which allows resolving particles even when near to each other. It is implemented in a microfluidics experiment allowing real-time multi-particle tracking at 70Hz, achieving a detection rate which exceeds 94% and only 1% false-detection.

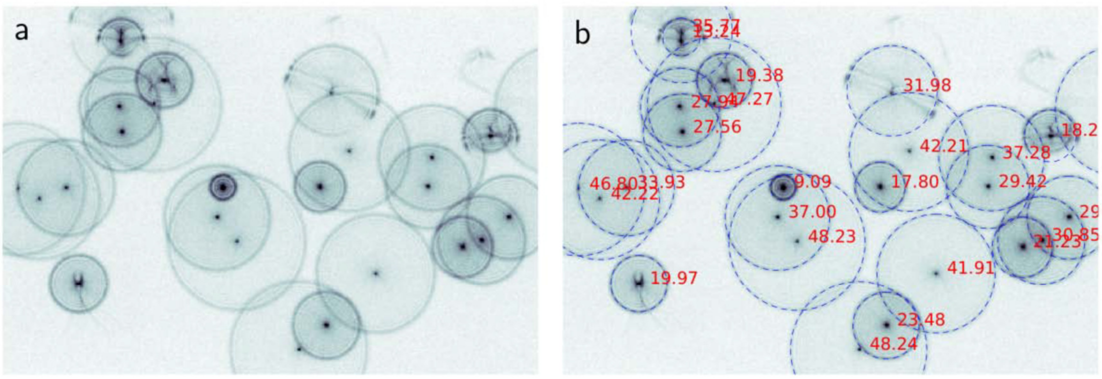

Fig. 1. Snapshots from the experiment demonstrating the algorithm robustness: (a) typical image complexity is exemplified in an unprocessed sub-frame consisting of 1/9 part of the full frame, corresponding to lateral dimension of 215×315 μm2. The axial range available for the particles is 140μm. (b) the corresponding analysis result; in red are the radii in pixels units.

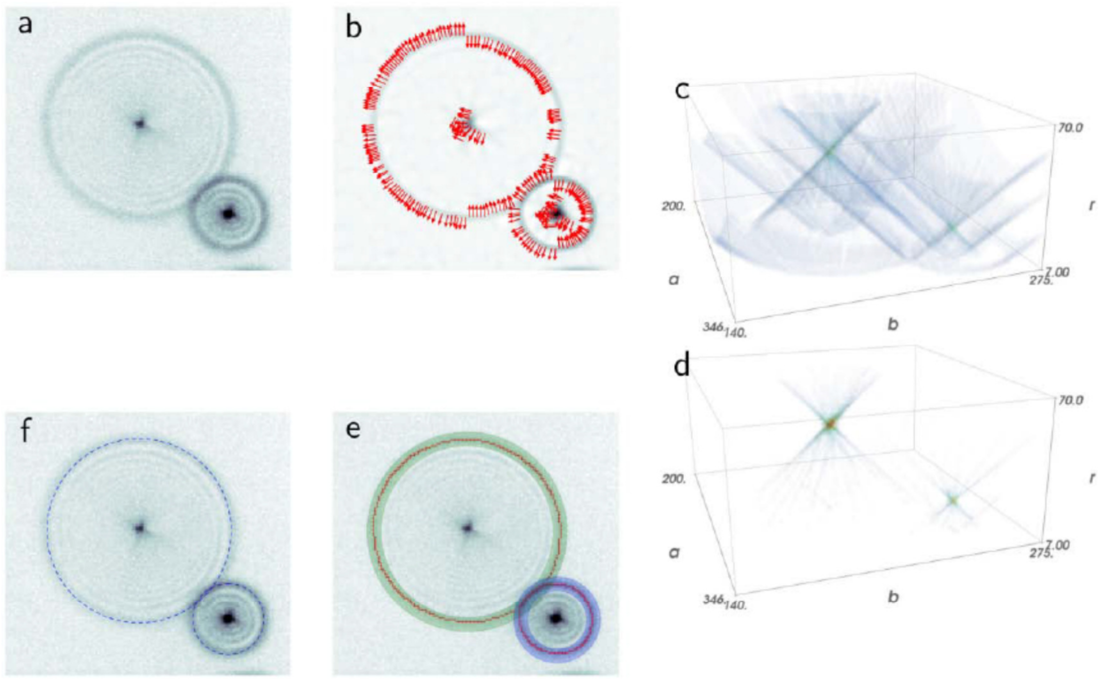

Fig. 2.: Algorithm outline: (a) raw sub-image containing two fluorescent particles; note that the inner rings of each particle are thinner than the outer most one. This scale separation admits suppression of all but the outer most ring via Gaussian smoothing; (b) ridge detection: the ridges are defined using a differential geometric descriptor and shown here as arrows representing X_- , the principal direction, corresponding to k_- , the least principal curvature, which is plotted in the background. The arrows originate from the ridge pixel. Note that the inner rings are successfully suppressed based on the scale separation. To ease visualisation every second detected ridge is omitted; (c) circle Hough transform: directed ridges → circle parameter space; (d) local maxima detection: radius dependent smoothing of the parameter space as well as normalisation by 1/r and thresholding greatly emphasise the local maxima representing the rings in the image; (e) sub-pixel accuracy: based on the detected rings, annulus masks (blue and green annuli in the figure) allow classification of ridge pixels (red points) and sub-pixel accuracy is achieved via circle fitting. Note the discarded directed ridges of the central peak (in (b)) as they do not belong to any local maxima in the processed circle parameter space (d); (f) the output: best fit circle for the ridge pixels of the outer-most ring of each particle.

Keywords
Pattern recognition, 3d particle tracking, fluorescence microscopy, micro-fluidics.

References

E. Afik, "Robust and highly performant ring detection algorithm for 3d particle tracking using 2d microscope imaging", e-print arXiv: 1310.1371

Acknowledgments
This work is supported by grants from the German-Israel Foundation (GIF) and the Lower Saxony Ministry of Science and Culture Cooperation (Germany).

A generalized view of high frequency substrate vibration induced wetting (Acoustowetting)

Ofer Manor[1,*], Amgad Rezk[2], James R. Friend[2] and Leslie Y. Yeo[2]
[1]*Chemical Engineering, Technion – Israel Institute of Technology*
[2]*Micro/Nanophysics Research Laboratory, RMIT University*

[*]manoro@technion.ac.il

High frequency surface vibrations, at frequencies comparable to HF and VHF radio frequencies O(1–100 MHz), may be used for generating flow at the micron and submicron scales. Such high frequency vibrations are generated by piezoelectric actuators, similar in shape to analog electronic signal filters that are commonly used in mobile phones, televisions, and other electronic devices. Transferring electric signals to mechanical momentum, these piezoelectric actuators excite different types of flow regimes, known in general as acoustic flow, when in contact with viscous fluids. Here we unravel a recently found wetting mechanism, observed in laboratory to be excited by high frequency vibrations in the form of piston-like substrate motion and surface acoustic waves (SAWs).

Active wetting is excited by vibration induced acoustic flow layer of submicron thickness near the three phase contact line of liquid/solid systems. This wetting effect further gives rise to various peculiarities including film spreading at different directions according with periodic stability of the film thickness, formation of wave pulse trains, SAW diffraction induced film fingering, etc. We show high frequency vibration induced wetting is governed by a generalized film equation that predicts the various physical peculiarities observed.

On the Effects of 3D Field Focusing at a Heterogeneous Permselective Surface on Concentration Polarization

Y. Green* and G. Yossifon

Faculty of Mechanical Engineering, Micro- and Nanofluidics Laboratory, Technion

*yoavgr@tx.technion.ac.il

Understanding the effects of 2D and 3D geometric field focusing effects at the interface of a microreservoir and a permselective surface (i.e. microchannel-nanochannel device) is of much importance in the growing field of electrokinetics and microfluidics. Such effects exist in numerous and varying experimental systems but little theoretical work has been conducted to better understand them. Previous studies made a number of oversimplifying assumptions regarding the geometry of the micro-/nano-fluidic device and its effects on concentration polarization so that the solution was valid only at certain limits. A 3D analytical solution is derived for an electrolyte undergoing concentration polarization within a *realistic* device geometry. The effects of both the microchannel and the nanochannel permselective interface's geometry are investigated. It is shown that limiting current transported through the permselective surface is not only a function of the area but is strongly geometry dependent (i.e. rectangular or square surface). Additionally, it is shown that there is an amplification of the current density with increased field focusing effects which stands in agreement with previous experimental results.

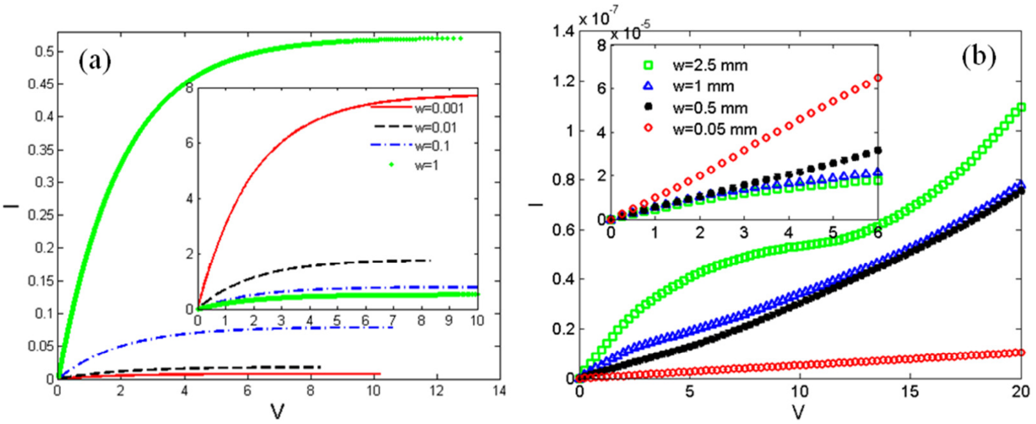

Fig. 1.: Computed non-dimensional current-voltage (I-V) curves for varying widths and constant permselective surface height. The inset shows the current density I/w . (b) Experimental I-V curves (in dimensional units) for nanochannels of varying widths were measured by Yossifon. et al(2010). Inset shows the same curves for the current density.

Keywords

Electrokinetic effects, Concentration-polarization, Ionic permselective interface

References

Rubinstein I., and Shtilman L., 1979, "Voltage against current curves of cation exchange membranes," J. Chem. Soc. Faraday Trans. 2, **75**, p. 231.

Rubinstein I., 1991, "Electroconvection at an electrically inhomogeneous permselective interface," Phys. Fluids Fluid Dyn., **3**(10), pp. 2301–2309.

Rubinstein I., Zaltzman B., and Pundik T., 2002, “Ion-exchange funneling in thin-film coating modification of heterogeneous electrodialysis membranes,” Phys. Rev. E, **65**(4), p. 041507.

Yossifon G., Mushenheim P., Chang Y.-C., and Chang H.-C., 2009, “Nonlinear current-voltage characteristics of nanochannels,” Phys. Rev. E, **79**(4), p. 046305.

Yossifon G., Mushenheim P., Chang Y.-C., and Chang H.-C., 2010, “Eliminating the limiting-current phenomenon by geometric field focusing into nanopores and nanoslots,” Phys. Rev. E, **81**(4), p. 046301.

Green Y., and Yossifon G., 2013, “Dynamical trapping of colloids at the stagnation points of electro-osmotic vortices of the second kind,” Phys. Rev. E, **87**(3), p. 033005.

Acknowledgments

This work was supported by ISF Grant No. 1078/10. We thank the Technion RBNI (Russell Berrie Nanotechnology Institute) for their financial support.

High-Order Numerical Simulations of Electrokinetic Instability in a Cross-shaped Microchannel

Q. Li[1], K. Anupindi[1], Y. Delorme[2] and S.H. Frankel[2,*]
[1]*School of Mechanical Engineering, Purdue University*
[2]*Faculty of Mechanical Engineering, Technion – Israel Institute of Technology*
[*]frankel@tx.technion.ac.il

Over the past two decades many integrated electrokinetic micro-devices have been developed as a key component for micro total analysis systems which integrate multiple laboratory processes and functions on a single platform. As the complexity of such systems increases, achieving robust control of the induced electrokinetic phenomena becomes increasingly important. Knowledge of electrokinetic instabilities (EKI) is desired in these electrokinetic micro-devices to trigger instabilities in applications like low Reynolds number micromixing or to suppress them in applications such as sample injection or separation where the minimum sample dispersion is needed.

An in-house high-order finite-difference incompressible Navier-Stokes solver, originally developed for large eddy simulation of transitional and turbulent flows (Shetty et al. 2010, Delorme et al. 2013a,b), is modified to incorporate the modified Ohmic model of Lin et al. (2004) for a symmetric binary electrolyte to enable EKI studies. The cross-shaped semi-circular channel geometry, initially treated as rectangular, is handling using a novel multiblock immersed boundary method (Anupindi et al. 2013). This will allow future simulations with arbitrarily complex geometries.

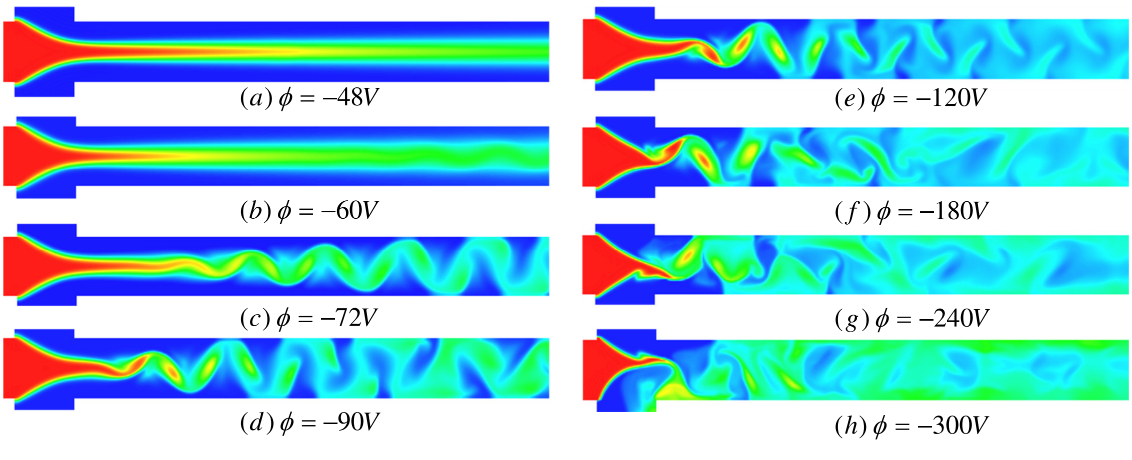

Fig. 1.: Preliminary results of representative instantaneous conductivity field snapshots of unstable electrokinetic flow in a cross-shaped microchannel. The electric potential imposed at the three inlets is from -48V to -300V, and the outlet of the channel is grounded (only close-up of junction and outlet shown).

Following the experimental study of Posner et al. (2006), a series of numerical simulations of convective instability of electrokinetic flows in a cross-shaped microchannel are performed. Figure 1 shows typical results for representative instantaneous conductivity field snapshots in the junction and outlet for unstable electrokinetic flow with centre-to-sheath conductivity ratio $\gamma = 3.5$ and applied field ratio of $\beta = 1.0$. For these flows Re is on the order of 0.1 and in these simulations $\mathrm{Re} \approx 0.3$. Despite low Re, EKI is observed and becomes more severe as the electric potential imposed at the inlets increases, which qualitatively agrees with the experimentally observed phenomena. Effects of varying the applied electric field, electric field ratio, and conductivity ratios on the EKI phenomena will be presented.

Keywords
Microfluidics, Electrokinetic instability, high-order methods, WENO scheme

References

Anupindi, K., Delorme, Y., Shetty, D., and Frankel, S. H., “A Novel Multiblock Immersed Boundary Method for Complex Arterial Hydrodynamics”, J. Comput. Phys., **254**, pp. 200-218, 2013.

Delorme, Y., Anupindi, K., Kerlo, A. E., Shetty, D., Rodefeld, M., Chen, J., and Frankel, S. H., “Large Eddy Simulation of Powered Fontan Hemodynamics”, J. Biomechanics, 46(2), pp. 408-422, 2013a.

Delorme, Y. T., Anupindi, K., and Frankel, S. H., “Large Eddy Simulation of FDA’s Idealized Medical Device”, Cardiovascular Engineering and Technology, in press, on-line access, 2013b.

Lin, H., Storey, B. D., Oddy, M. H., Chen, C. H., and Santiago, J. G., “Instability of electrokinetic microchannel flows with conductivity gradients”, Physics of Fluids, 16:1922, 2004.

Posner, J. D. and Santiago, J. G., “Convective instability of electrokinetic flows in a cross-shaped microchannel”, Journal of Fluid Mechanics, 555(1):1–42, 2006.

Shetty, D., Fisher, T., Chunekar, A., and Frankel, S. H., "High-Order Incompressible Large Eddy Simulation of Fully Inhomogeneous Turbulent Flows", Journal of Computational Physics, 229(23), pp. 8802-8822, 2010.

Frequency dispersion in dipolophoresis of metallodielectric Janus spheres.

Alicia Boymelgreen[1,*], Gilad Yossifon[1] and Touvia Miloh[2]
[1] *Mechanical Engineering, Technion*
[2] *Mechanical Engineering, Tel Aviv University*
[*]aliciab@tx.technion.ac.il

Dipolophoresis (DIP) is an umbrella term for the two non-linear electrokinetic phenomenon of induced-charge electrophoresis (ICEP) and dielectrophoresis (DEP). It has previously been shown that this effect is responsible for the obtainment of a finite velocity by "metallodielectric" Janus spheres – comprised of one conducting and one dielectric hemisphere - even under the application of a uniform AC field [1-3]. At low frequencies, this mobility is dominated by induced-charge effects, wherein the stronger induced-charge electroosmotic flow around the polarizable hemisphere propels the particle perpendicular to the electric field in the direction of its dielectric end. Surprisingly, it was observed that this motion is at a maximum for applied frequencies in the range of 1kHz, beyond which the effect decays. Here we examine the influence of varying experimental conditions including electrolyte concentration and particle size on this limit. Additionally, we present for the first time an analytical solution which is capable of predicting this optimum based on our previous formulation of the mobility of a metallodielectric Janus sphere which is uniquely valid for arbitrary electric double layer length [3]. This work is of both fundamental and practical importance and may be used to optimize the behavior of Janus micromotors or carriers in lab-on-a-chip analysis systems

Keywords
Janus, dipolophoresis, induced-charge electrophoresis, micro/nano fluidics

References

[1] TM Squires, MZ Bazant, "Breaking symmetries in induced-charge electroosmosis and electrophoresis", Journal of Fluid Mechanics (2006)

[2] S. Gangwal, O. J. Cayre, M. Z. Bazant, and O. D. Velev, "Induced-charge electrophoresis of metallodielectric Janus particles", Physical Review Letters (2008)

[3] A.M Boymelgreen and T. Miloh, "Alternating current induced-charge electrophoresis of leaky dielectric Janus particles", Physics of Fluids (2012)

Acknowledgments
The authors would like to acknowledge US-Israel Binational Science Foundation Grant [2009371]. The Janus particle preparation was possible through the financial and technical support of the Technion RBNI (Russell Berrie Nanotechnology Institute) and MNFU (Micro Nano Fabrication Unit).

Dispersion Phenomena of Fine Particles in Pulmonary Alveolar Capillary-Inspired Networks

H. Stauber[1,*], R. Fishler[1], P. Hofemeier[1], D. Waisman[2, 3], and J. Sznitman[1]
[1]*Department of Biomedical Engineering, Technion - Israel Institute of Technology*
[2]*Rappaport Faculty of Medicine, Technion - Israel Institute of Technology*
[3]*Department of Neonatology, Carmel Medical Center*

hagitstauber@gmail.com

Microcirculation in alveolar capillary networks (ACN) is typically described by classic analytical models such as the "sheet flow" model[1],due to the resemblance of the capillary mesh to a pattern of repeating hexagonal structures when spread flat in 2D (Fig.1a). Using computational fluid dynamics (CFD), we investigate generic planar 2D models of alveolar capillary networks to gain quantitative insight into the transport mechanisms governing fine micron and sub-micron particles in ACN-like geometries; such particles are known to potentially translocate from the lungs into the pulmonary microcirculation [2,3]. Our simulations are confined to studying the specific influence of the ACN geometry, where the dynamics of red blood cells are not accounted. We conduct Lagrangian tracking of injected particles ranging from 10 nm to 1µm (including massless particles), under the combined influence of convection and Brownian diffusion, with Peclet numbers spanning Pe = 60 to $6{\cdot}10^3$. We modulate the capillary diameter in the ACNs (~5 to11µm), giving rise tovarious levels of the effective perfused area (66%-84%), where perfusion velocities are matched to physiologically-realistic conditions[4] (Re~$3{\cdot}10^{-3}$).We discuss the dynamics of particle transport in ACNs by extracting temporal statistics for ensembles of particles (e.g., mean square displacement)

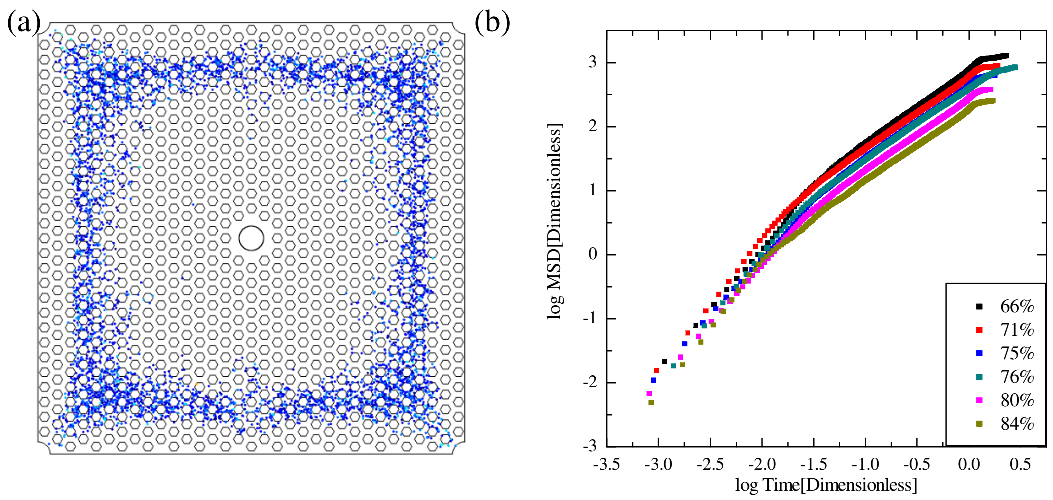

Fig.1: (a) Schematic of a 2D alveolar capillary network model with hexagon-shaped posts representative of 20 alveoli(348µm×353µm). Snapshot illustrates 1 µm diameter particles (n=5000) released after t=10.8 sec from the arteriole(inlet center circle)and traveling towards draining venules (corner outlets). (b) Log-log plotsof MSD curves for 1 µm diameter particlesfor different levels of perfused area (%).Results are non-dimensional, MSD was non-dimensionalized by square capillary diameter and time by $T_{0,}$ initial time of losing particles from specific geometry.

Our results indicate thatregardless of size, particles are mainly affected by convection during the initial phase (slope of ~2),while diffusional transport plays an increasing role over longer time scales, where slopes gradually decrease to a value of approximately 1(Fig.1b). In particular, we find that capillarydiameter (or effective perfusion area) plays a major role in enabling dispersion bydelimiting streamline patterns, and thus affecting the possible pathways of particles, such that the narrower the capillary the higherprobability for a particle to follow existing trajectories. Overall, our findings suggest that the ACN morphology play a leading role in determining the transport characteristics of particles, relative to the intrinsic dynamics of the particles.

Keywords
Microcirculation, Dispersion, Particle Transport, Mean Square Displacement, Diffusion.

References

[1] Fung, Y. C. & Sobin, S. S. Theory of sheet flow in lung alveoli. *J. Appl. Physiol.***26,** 472–488 (1969).
[2] Choi, H. S. *et al.* Rapid translocation of nanoparticles from the lung airspaces to the body. *Nat. Biotechnol.***28,** 1300–1303 (2010).
[3] Oberdörster, G. *et al.* Translocation of Inhaled Ultrafine Particles to the Brain. (2008). at
[4] Popel, A. S. & Johnson, P. C. Microcirculation and Hemorheology. *Annu. Rev. Fluid Mech.***37,** 43–69 (2005).

Acknowledgments
The authors would like to express appreciation for the support of the sponsors MANLAM Fund for Cardiology Research, Technion.

Nanodroplet array for multiplexed single-cell assays

J. Shemesh[1,2,*], T. Ben Arye[1,2], J. Avesar[1], J. H. Kang[3,4], A. Fine[1], M. Super[3], A. Meller[1,2], D. E. Ingber[3-5], S. Levenberg[1,2]

[1]*Department of Biomedical Engineering, Technion*
[2]*Russell Berrie Nanotechnology Institute, Technion*
[3]*Wyss Institute for Biologically Inspired Engineering, Harvard University*
[4]*Harvard School of Engineering and Applied Sciences*
[5]*Vascular Biology Program, Boston Children's Hospital, and Harvard Medical School*

[*]javesar@tx.technion.ac.il

Microfluidic water-in-oil droplets that serve as separate, chemically isolated compartments can be applied for single-cell analysis; however, to effectively investigate encapsulated cells over prolonged time periods, droplets must remain stationary, which remains difficult. We present a platform which generates a stationary nanodroplet array (SNDA) using nanowells branching off of a main microfluidic channel. It is operated by a unique and unconventional loading procedure, in which the dispersed medium is injected first and sheared into droplets before a continuous liquid phase is injected to sheath the droplets, eliminating the need for fine pressure control or external tubing. Using this approach, we present the ability to continuously monitor the metabolic activity of single cells over time, and to determine the concentration of viable pathogens in blood derived samples directly by measuring the number of colony-formed droplets. The method is simple to operate, requires a few microliters of reagent volume, and is portable. This technology may be particularly useful for multiplexed assays where prolonged and simultaneous visual inspection of many isolated single cells is required.

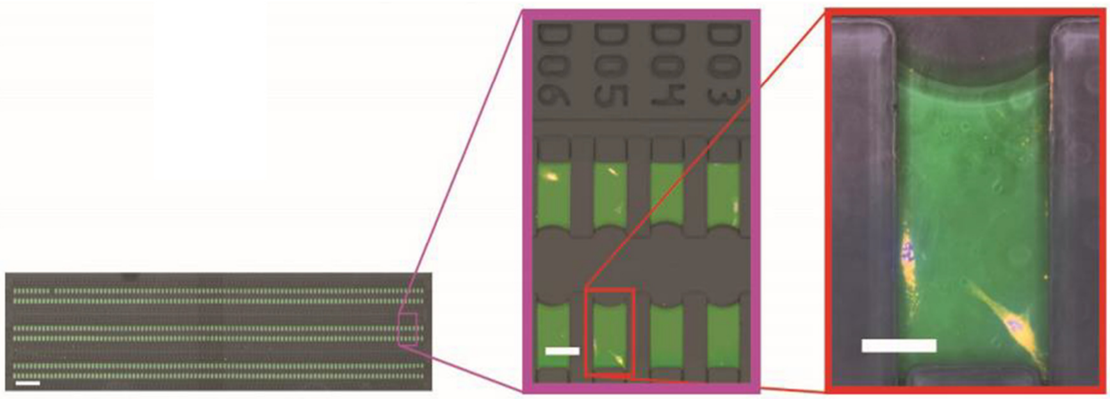

Fig. 1.: An SNDA holding droplets of medium containing FITC-dextran and fibroblasts visualized at three different magnifications. Hoechst 33342 and DiI were used to stain the cell membrane and nucleus. Each magnification was constructed by two separate images. Scale bars, 2mm, 200µm, 100µm.

Dynamics of an Elastic Cylinder Containing a Viscous Liquid with Application to Soft Robotics

S.B. Elbaz* and A.D. Gat
Faculty of Mechanical Engineering, Technion – Israel Institute of Technology
*shaibaz@tx.technion.ac.il

Viscous flows within a solid body apply both pressure and shear stress at the solid-liquid interface and thus create stress- and deformation-fields within the solid structure, which in turn affect the flow field. The interaction between low-Reynolds-number liquid flows and elastic deformation of solid-structures is applicable to various research fields such as instabilities in micro-fabrication processes, self-folding of solid sheets (commonly referred to as capillary origami), densification of patterned arrays of carbon nanotubes, self-assembly and modification of the mechanical and geometrical properties of arrays of solid structures and soft robotics (Shepherd *et al.* 2013).

The current study brings forth an analysis of elasto-viscous driven deformation diffusion of an axi-symmetric shell containing a viscous liquid. The aim of this work is to apply models and methods used in the study of biological flows to study time varying deformation patterns in soft robotics. The interaction between fluid and solid dynamics for the case of viscous flow through elastic cylinders was extensively studied in the context of collapsible tubes (Heil 1998), the study of pipes conveying fluid (Paidoussis 1998) and arterial blood flows. The novelty of our research emanates from the study of the external stress applied on the cylinder and our focus on phenomena with a characteristic time scale of the order-of-magnitude of the viscous-elastic interaction.

We study the interaction between elastic slender axi-symmetric structures, subject to external stress and induced pressure boundaries, and internal time-varying viscous flows. We neglect inertia in the liquid and solid and focus on the flow through a thin-walled slender elastic cylinder either closed at one end (see Figure 1) or open at both and containing a base flow. We obtain an inhomogeneous linear diffusion equation governing the deformation field, where the derivative of the pressure at either boundary appears as a source within the equation. This research may prove valuable to applications such as micro-swimmers and soft-robotics by allowing for the design and control of a time-varying deformation field, in turn enabling propulsion and navigation of the robot/vehicle.

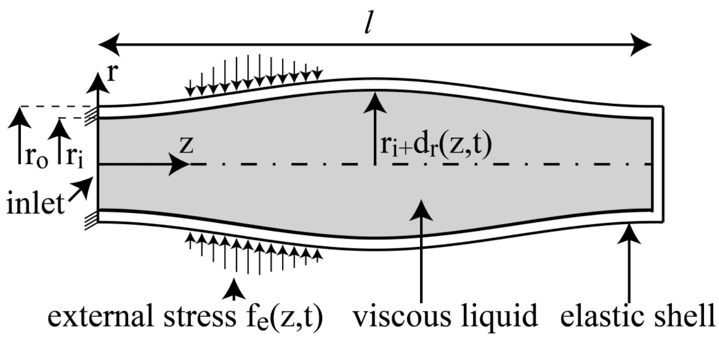

Figure 1: A schematic description of the elastic shell and the coordinate system.

Keywords
Viscous flows, fluid-structure interaction.

References

Heil, M. 1998 Stokes flow in an elastic tube – a large-displacement fluid-structure interaction problem. Int. J. Num. Methods in Fluids **28**, 243–265.

Padoussis, MP 1998 Fluid-Structure Interactions, Slender Structures and Axial Flow. Academic Press, London.

Shepherd, Robert F, Stokes, Adam A, Freake, Jacob, Barber, Jabulani, Snyder, Phillip W, Mazzeo, Aaron D, Cademartiri, Ludovico, Morin, Stephen A & Whitesides, George M 2013 Using explosions to power a soft robot. *Angewandte Chemie* **125** (10), 2964–2968.

Acknowledgments
This research was supported by the ISRAEL SCIENCE FOUNDATION (Grant No. 818/13)

Frame Rate Free Image Velocimetry for Microfluidic Devices

E. Keinan[1,+,*], Elishai Ezra [1,+], Yaakov Nahmias [1,2]

[1]*Center for Bioengineering, Benin School of Computer Science and Engineering, The Hebrew University of Jerusalem*

[2]*Department of Cell and Developmental Biology, Silberman Institute of Life Sciences, The Hebrew University of Jerusalem*

[+]Authors contributed equally

[*]eliezer.keinan@mail.huji.ac.il

Experimental quantification of fluid velocity is an important component in the interdisciplinary field of microfluidics. The resolution of current velocimetry methods, such as Particle Tracking Velocimetry (PTV) is limited by both frame rate and exposure time. Here we introduce Streamline Image Velocimetry (SIV), a method to derive fluid velocity fields in fully developed laminar flow from long-exposure images of streamlines. Streamlines confine streamtubes, in which the volumetric flow is constant for incompressible fluid. Using an explicit analytical solution as a boundary condition, velocity fields and emerging properties such as shear force and pressure can be quantified throughout. Numerical and experimental validations show a high correlation between anticipated and measured results, with $R^2 > 0.91$. We report spatial resolution of 2 μm in a flow rate of 0.15 m/s, resolution that can only be achieved with 75 kHz frame rate in traditional PTV. SIV can be used for higher flow rates in the same spatial resolution, as long as the immersed particles visualize the fluid streamlines. Furthermore, while in PTV the error related to Brownian motion increases with frame rate increase, in SIV the Brownian motion is averaged due to long exposure time in streamline imaging. Streamlines can be continuously visualized in microfluidic devices with complex boundary conditions such as porous elements. We demonstrate the calculation of shear stress near implanted carbon nano-tube porous pillars in microfluidic channel using streamlines visualization. SIV is simple and quick and can be used for a range of applications ranging from *in vivo* study of hemodynamics to the design of complex microfluidic circuits.

Acinus-on-a-chip: a microfluidic platform for pulmonary acinar flows

R. Fishler, M.K. Mulligan, and J. Sznitman*
Department of Biomedical Engineering, Technion

*sznitman@bm.technion.ac.il

Convective respiratory flows in the pulmonary acinus and their influence on the fate of inhaled particles are typically studied using computational fluid dynamics (CFD) or scaled-up experimental models. However, current experiments generally capture only flow dynamics, without inhaled particle dynamics due to challenges in simultaneously matching the dimensionless numbers for flow (e.g., Reynolds and Womersley number) and for particles (e.g., Stokes and gravity numbers). In an effort to overcome these limitations, we introduce a novel microfluidic device mimicking acinar flow conditions directly at the alveolar scale. The model features an anatomically-inspired acinar geometry with five dichotomously branching airway generations lined with periodically expanding and contracting alveoli. using micro-particle image velocimetry within the device we reveal experimentally for the first time a gradual transition of alveolar flow patterns along the acinar tree from recirculating to radial streamlines (Fig. 1), in support of hypothesized predictions from CFD simulations. We further use the device to visualize deposition sites of airborne fluorescent micro-particles (0.1-1µm) and real-time trajectories of airborne incense particles inside the system. This platform serves as a powerful in vitro tool for investigating the mechanisms of particle deposition deep in the lung.

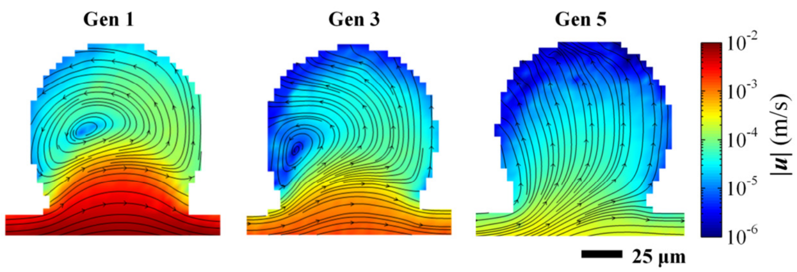

Fig. 1. Particle image velocimetry results at device generations 1, 3 and 5

Keywords
lungs, pulmonary acinus, respiratory flows, flow visualization, PIV

References

Fishler, Rami, Molly K. Mulligan, and Josué Sznitman. "Acinus-on-a-chip: A microfluidic platform for pulmonary acinar flows." *Journal of Biomechanics* (2013).

Acknowledgments
The authors would like to express appreciation for the support of the European Commission (FP7 Program) through a Career Integration Grant (PCIG09-GA-2011-293604), the Israel Science Foundation (Grant nr. 990/12) and the Technion Center of Excellence in Environmental Health and Exposure Science (TCEEH). Microfabrication of microfluidic chips was conducted at the Micro-Nano Fabrication Unit (MNFU) of the Technion and supported by a seed grant from the Russel Berrie Institute of Nanotechnology (RBNI) at Technion.